Evolving spherical Boson Stars on a 3D cartesian grid

F. Siddhartha Guzmán*

Max Planck Institut für Gravitationsphysik, Albert Einstein Institut, Am Mühlenberg 1, 14476 Golm, Germany.
Center for Computation and Technology, 302 Johnston Hall,
Louisiana State University, Baton Rouge, LA 70803.†

(Dated: August 2, 2004)

A code to evolve boson stars in 3D is presented as the starting point for the evolution of scalar field systems with arbitrary symmetries. It was possible to reproduce the known results related to perturbations discovered with 1D numerical codes in the past, which include evolution of stable and unstable equilibrium configurations. In addition, the apparent and event horizons masses of a collapsing boson star are shown for the first time. The present code is expected to be useful at evolving possible sources of gravitational waves related to scalar field objects and to handle toy models of systems perturbed with scalar fields in 3D.

PACS numbers: 04.40.-b, 04.25.Dm, 04.30.Db

I. INTRODUCTION

Boson Stars (BSs) are localized, regular, spherically symmetric solutions of Einstein's field equations, whose matter content is provided by a complex scalar field with mass and self-interaction [1, 2, 3]. Recently Boson Stars have appeared in many contexts. Traditionally they were proposed to be alternatives of compact objects [1, 3]; they have been proposed as candidates for dark matter [4]; this includes the possibility to emulate galactic supermassive Black Holes [5]; they have even been considered as sources of gravitational waves [6]; and they have been used in the field of numerical relativity to test evolution formulations of Einstein's equations and experience with gauge conditions [7], since these objects are very tractable in the sense that they have no defined surface and their dynamics do not tend to form shocks, and therefore sophisticated techniques -like shock capturing methods- are not required. Moreover, BSs define sequences of equilibrium configurations which serve to test a numerical implementation. That is, for a spherical equilibrium configuration the field has to oscillate with a constant frequency while the geometry of the space-time has to remain static. For general reviews in BSs see [8, 9]. In this paper I focus on numerical challenges, and set up a starting point to study the astrophysical applications mentioned before. Instead of developing the original mean field approximation to calculate the expectation value of the stress-energy tensor components of a quantum scalar field as done originally [1, 2], the field is simply considered to be classical as usually done when studying the evolution of these systems.

For several reasons, such systems have only been evolved for long times (long enough to observe the oscillations of a perturbed star) in spherical symmetry using 1D codes [10, 11, 12]. The main reason for this is without doubt the difficulty in formulating the evolution equations for the space-time from Einstein's equations when using non-spherical symmetry. In spherical symmetry these evolution equations are replaced with the slicing condition and the constraints (see for instance [11, 12]). The resulting ODEs can be integrated at each time step during the evolution, which is computationally cheap and allows a constrained evolution under control for very long periods of time. Other problem in higher dimensions is the difficulty to achieve the same resolutions used in 1D simulations due to the lack of computational resources, since the memory requirements in 3D unigrids forces one to sacrifice either the size of the physical domain or the numerical resolution in regions where the gravitational field still strong. Moreover, the number of variables in higher dimensions is also bigger than in 1D.

The practical concern is that in 3D the constraint equations are elliptic, which one does not want to solve at every time step due to the extreme hardware requirements needed to carry out a significantly long simulation. Therefore it is usually preferable to use unconstrained gauges and evaluate the constraints just to monitor the accuracy and convergence of the solution one is calculating. Even though unconstrained evolutions of Einstein's equations are still under study, it is known that some formulations work better than others when using certain gauge conditions. In this paper the BSSN formulation of general relativity is considered [13], which has shown to be more stable for longer evolutions than the ADM formulation for a number of physical systems [7] and presents different stability properties [14] (for test beds and comparisons under different gauges see [15]).

The Lagrangian density from which the Einstein and

*E-mail: guzman@cct.lsu.edu
†Current address.

Klein-Gordon equations describing BSs are derived reads:

$$\mathcal{L} = -\frac{R}{16\pi G} + g^{\mu\nu}\partial_\mu\phi^*\partial_\nu\phi + V(|\phi|^2), \qquad (1)$$

where R is the Ricci scalar, ϕ is a complex scalar field minimally coupled to gravity, ϕ^* is its complex conjugate and V the potential of self-interaction of the field. The resulting Einstein's equations are $G_{\mu\nu} = 8\pi G T_{\mu\nu}$, provided the stress energy tensor is

$$T_{\mu\nu} = \frac{1}{2}[\partial_\mu\phi^*\partial_\nu\phi + \partial_\mu\phi\partial_\nu\phi^*] - \frac{1}{2}g_{\mu\nu}[\phi^{*,\alpha}\phi_{,\alpha} + V(|\phi|^2)]. \qquad (2)$$

The equation satisfied by the scalar field can be obtained either from the Bianchi identities or by directly using the variational principle on (1), which for the present case reduces to the Klein-Gordon equation on the space-time background,

$$\left(\Box - \frac{dV}{d|\phi|^2}\right)\phi = 0 \qquad (3)$$

where $\Box\phi = \frac{1}{\sqrt{-g}}\partial_\mu[\sqrt{-g}g^{\mu\nu}\partial_\nu\phi]$, based on the corresponding line element:

$$ds^2 = -\alpha(\mathbf{x},t)^2dt^2 + \gamma_{ij}(\mathbf{x},t)(dx^i+\beta^i dt)(dx^j+\beta^j dt) \qquad (4)$$

where latin indices stand for the spatial coordinates and $\mathbf{x}$ indicates dependence on all spatial (cartesian) coordinates, α is is the lapse function, β^i the shift vector and γ_{ij} is the 3-metric in the 3+1 decomposition of the space-time. As I am going to deal only with spherically symmetric Boson Stars, a zero shift is used for stable equilibrium configurations, and a simple but sophisticated driver involving a non-zero shift will prove to be necessary in order to follow the evolution of unstable configurations. The general form of the potential to be studied here is $V(|\phi|) = \frac{1}{2}m^2|\phi|^2 + \frac{\lambda}{4}|\phi|^4$, which has been the most studied case with 1D codes [10, 11, 12], among a variety of potentials studied [16, 17, 18] and others including very general non polynomial potentials [19].

With this notation in mind in section II the numerical techniques used in the simulations shown are described. In section III physical tests are presented and a set of production runs from which the frequencies of the oscillation modes found in 1D for several configurations are reproduced with the present 3D code. In section IV an example of various unstable BSs is shown. A trick to excite non-radial modes is presented in section V through the manipulation of the refinement of the grid in different directions. Section VI refers to the restrictions of the present code. Finally, some comments are addressed in section VII.

II. NUMERICAL METHODS

A. Evolution in time

The scalar field is described by its real and imaginary parts, such that $\phi(\mathbf{x},t) = \phi_1(\mathbf{x},t) + i\phi_2(\mathbf{x},t)$. I define four new real variables based on combinations of derivatives of the scalar field as follows: $\pi_1 + i\pi_2 := \frac{\gamma^{1/2}}{\alpha}(\partial_t\phi - \beta^i\partial_i\phi)$, and $\psi_{1a} + i\psi_{2a} := \partial_a\phi$ for $a = x, y, z$, where α is still the lapse function of the space-time and γ is the determinant of the three metric γ_{ij}. In terms of these new variables the KG equation (3) can be rewritten as a set of first order evolution equations:

$$\partial_t\psi_{1a} = \partial_a\left(\frac{\alpha}{\gamma^{1/2}}\pi_1 + \beta^i\psi_{1i}\right) \qquad (5)$$

$$\partial_t\pi_1 = \partial_i\left(\alpha\gamma^{1/2}\gamma^{ij}\psi_{1j} + \beta^i\pi_1\right) - \frac{1}{2}\alpha\gamma^{1/2}\frac{\partial V}{\partial|\phi|^2}\phi_1 \qquad (6)$$

$$\partial_t\psi_{2a} = \partial_a\left(\frac{\alpha}{\gamma^{1/2}}\pi_2 + \beta^i\psi_{2i}\right) \qquad (7)$$

$$\partial_t\pi_2 = \partial_i\left(\alpha\gamma^{1/2}\gamma^{ij}\psi_{2j} + \beta^i\pi_2\right) - \frac{1}{2}\alpha\gamma^{1/2}\frac{\partial V}{\partial|\phi|^2}\phi_2 \qquad (8)$$

where the summation convention is assumed over latin indices. Evidently the set (5-8) is a system of evolution equations that provides the derivatives of the scalar field at each time slice, from which it is possible to reconstruct the scalar field itself using the definition of π_1 and π_2. When solving the KG system above, it is necessary to solve the evolution Einstein's equations in the BSSN formulation as described in reference [13]. Basically the BSSN formulation uses the evolution variables: $\Psi = \ln(\det\gamma_{ij})/12$, $\tilde{\gamma}_{ij} = e^{-4\Psi}\gamma_{ij}$, $K = \gamma^{ij}K_{ij}$, $\tilde{A}_{ij} = e^{-4\Psi}(K_{ij} - \gamma_{ij}K/3)$ and $\tilde{\Gamma}^i = \tilde{\gamma^{jk}}\Gamma^i_{jk}$, instead of the usual ADM variables γ_{ij} and K_{ij}. The evolution equations for the new variables are described in a number of references, e.g. [13].

The integration of the Klein-Gordon equation (5-8) and the BSSN variables is performed using the method of lines with second order centered differencing in space. For the time integration a third order Runge-Kutta (RK3) algorithm is used [20].

B. Gauge choice

In the case of stable equilibrium configurations the evolution of the gauge was carried out using zero shift and the $1 + \log$ slicing condition [22], which is a particular method according to which the lapse evolves as

$$\partial_t\alpha = -2\alpha(K - K_0) \qquad (9)$$

where K is the trace of the extrinsic curvature and $K_0 = K(t = 0)$ (K_0=0 in the present case). Due to the time independence of the metric one knows *a priori* that $K_{ij} = -\frac{1}{2\alpha}\partial_t\gamma_{ij} = 0$, i.e. that K has to be zero for equilibrium configurations of boson stars. However this is only valid in the continuum limit. In practice, the discretized version of the equations will prevent the extrinsic curvature from being exactly zero. Nevertheless it was observed that the components of the extrinsic curvature converged to such value.

In order to evolve unstable equilibrium configurations the 1+log slicing condition was also used, but it was necessary an additional hyperbolic gamma-driver shift condition [22]. This type of conditions are necessary after a black hole has formed and prevent the grid stretching effect followed by an unphysical growth of the horizon. As described in [22], such gamma-drivers are diverse, but for the spherically symmetric case I deal with here, the following hyperbolic condition was used:

$$\partial_t\beta^i = \frac{3}{4}\alpha^p B^i \ , \quad \partial_t B^i = \partial_t\tilde{\Gamma}^i - \eta B^i \tag{10}$$

where p and η are coefficients controlling the gauge speeds and certain damping added to the shift respectively.

C. Exterior Boundary Conditions

A modified version of radiative boundary conditions is applied to the BSSN variables and to the defined first order variables ϕ, ψ and π. For all these variables it is assumed that they behave as a constant plus an outgoing radial wave at the boundaries, plus an extra term that helps to control initial transient effects, that is

$$f(\mathbf{r}, t) = f_0 + u(r - t)/r + h(t)/r^n \tag{11}$$

where $r = |\mathbf{r}|$, f_0 is one for the lapse and the diagonal components of the three metric and zero otherwise, $h(t)$ is a function of t and n an unknown power. The reason to choose the outgoing radial wave boundary condition is that it has proved to be very efficient at absorbing waves. The differential equation in Cartesian coordinates corresponding to the expression above is

$$\frac{x_i}{r}\partial_t f + \partial_i f + \frac{v x_i}{r^2}(f - f_0) \simeq \frac{x_i h'(t)}{r^{n+1}}. \tag{12}$$

For a given n, the unknown function $h'(t)$ can be evaluated at a point away from the boundary, and substituted in the previous equations to evaluate any dynamical variable at the boundary [22]. It was found that when the potential of the scalar field has zero self-interaction ($\lambda = 0$), then switching off the extra term ($h = 0$), that is, using standard radiative boundary conditions, the evolution behaves properly. Nevertheless, when the self-interaction is non zero, it was found that a bigger power ($n = 3$ or $n = 5$) prevents a pulse on the field variables coming from the boundaries. It is worth mentioning that instead of using a sponge as used in spherically symmetric evolutions with $\lambda \neq 0$ [11], the modifications mentioned here sufficed to evolve the shown systems with second order accuracy for a number of crossing times. Finally it is important to stress that in the case of spherical symmetry these BCs are appropriate. More care is required when systems with other symmetries are studied, since this approximation is only valid if one considers that the front signals propagating outwards are spherical.

D. Interior Boundary Conditions

After an apparent horizon has been found for the first time, a lego sphere (the set of points of a cubic grid contained inside a 2-sphere) is excised from its interior. Excising is a common practice when evolving black hole space-times [21, 22, 23, 24] and has shown to be an essential strategy when evolving matter fields as shown recently in [25, 26]; the main aim of using excision is that the code is not forced to calculate quantities in a region close to a singularity, where gradients are expected to be inaccurate. In the present case one expects the matter field to fall into the resulting horizon in a finite time, thus the excision region is allowed to resize according to the size and shape of the apparent horizon. For this purpose the apparent horizon finder in [27] was used every time step. A buffer zone of five points between the excision region and the apparent horizon is kept.

The interior boundary is the set of points delimiting the excision region. As apparent horizons lie inside event horizons, all the signals propagate towards the excision region and so do the errors. This is the reason why the time derivative of all the evolved variables is set to be zero at the the inner boundary. The implementation consists of calculating the time derivatives of the variables one point away from the excision region in the direction determined by the normal; this time derivative is then used to evolve the variable on the excision boundary.

III. TESTS ON THE STABLE BRANCH

A. Initial Data

In order to test the evolution code, the first important issue is setting up initial data that work in 1D. For this, the well studied case of spherically symmetric equilibrium configurations is chosen, where the scalar field os-

cillates with constant frequency whereas the geometry in the chosen gauge remains time-independent. Einstein's equations are solved on a spherically symmetric background by assuming that the space time is static and that the scalar field has the form $\phi(r,t) = \varphi(r)e^{i\omega t}$, so that all the components of the stress-energy tensor are time-independent. Assuming $ds^2 = -\alpha(r)^2dt^2 + a(r)^2dr^2 + r^2d\Omega^2$ one arrives at the equations

$$\begin{aligned} \frac{a'}{a} &= \frac{1-a^2}{2r} + \frac{1}{4}\kappa r\left[\omega^2\varphi^2\frac{a^2}{\alpha^2} + \varphi'^2 + a^2V\right] \qquad (13)\\ \frac{\alpha'}{\alpha} &= \frac{a^2-1}{r} + \frac{a'}{a} - \frac{1}{2}\kappa r a^2 V \\ \varphi'' &+ \varphi'\left(\frac{2}{r} + \frac{\alpha'}{\alpha} - \frac{a'}{a}\right) + \omega^2\varphi\frac{a^2}{\alpha^2} - a^2\frac{dV}{d|\varphi|^2}\varphi = 0 \end{aligned}$$

which is a set of coupled ordinary differential equations to be solved under the conditions $a(0) = 1$, $\varphi(0)$ finite and $\varphi\prime(0) = 0$ in order to guarantee regularity and spatial flatness at the origin, and $\varphi(\infty) = \varphi\prime(\infty) = 0$ in order to ensure asymptotic flatness at infinity as described in [1, 10, 11, 28]. Here $\kappa = 8\pi G$. The solution was calculated using the standard rescaled variables $\varphi = \sqrt{4\pi G}\varphi$, $r = mr$, $t = \omega t$, $\alpha = \frac{m}{\omega}\alpha$ and $\Lambda = \frac{\lambda}{4\pi G m^2}$ so that the coordinate time is given in units of $1/\omega$ and the distance in units of $1/m$. In Fig. 1 the sequence of equilibrium configurations corresponding to different self-interaction values is shown, and will serve to illustrate the functionality of this 3D code.

Once the system (13) has been solved with sufficiently high resolution, the straightforward identification of the 1D variables with the 3D variables at initial time is as follows: $\alpha(\mathbf{x},0) = \alpha(r)$, $\sqrt{\gamma_{rr}(\mathbf{x},0)} = a(r)$, $\phi_1(\mathbf{x},0) = \varphi(r)$, $\phi_2(\mathbf{x},0) = 0$, $\pi_1(\mathbf{x},0) = 0$ and $\pi_2(\mathbf{x},0) = \frac{a}{\alpha}\varphi(r)$. This can be easily understood just by recalling the *ansatz* $\phi(r,t) = \varphi(r)e^{it}$ in rescaled units. Then the 3D cartesian grid is populated by copying the values of such variables to the nearest neighbor grid points of the 3D domain, and applying the coordinate transformation from spherical to cartesian coordinates. Since it is known *a priori* that the space time should be time-independent I set the components of the extrinsic curvature to zero initially. Then the unconstrained evolution is started and the geometry and the field evolve according to their corresponding equations.

B. Convergence

The convergence of a non vacuum system is a major issue for many reasons. The usually applied boundary conditions to the geometrical quantities correspond to outgoing waves and moreover the boundary conditions for the scalar field with a potential term have no reported solution up to now for a 3D grid, so that

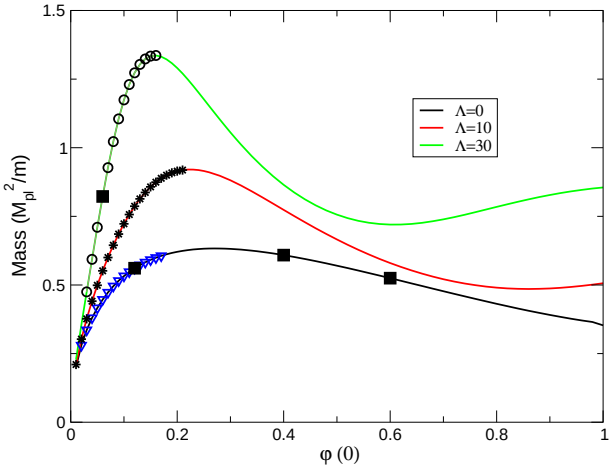

FIG. 1: The sequences of equilibrium configurations are shown for different values of the self-interaction coefficient Λ. The configurations to the left of the respective peaks are stable configurations, and those to the right are unstable, which means that either they could collapse to form black holes or disperse away under infinitesimal perturbations, depending on the sign of the binding energy (see below). The triangles down, the stars and the circles correspond to the configurations evolved to trace the radial modes of oscillation of stable configurations. The filled squares represent four particular cases studied in depth to show the capabilities of the numerical techniques.

the boundary conditions are not necessarily consistent with the evolution equations; these difficulties are not particular to the present problem, but are also a concern when solving the vacuum Einstein's equations or relativistic hydrodynamical fields, because these conditions could allow constraint violating modes to come into the domain and destroy the simulations. Nevertheless it was found that the modified Sommerfeld boundary conditions mentioned in the previous section, work well for the variables describing the field and the geometric quantities at once for quite a long time. In Fig. 2 it is shown the convergence of the L_2 norm of the violation of the Hamiltonian constraint produced for two initial configurations. Second order convergence is manifest indicating the accurate and stable behavior of the simulations for dozens of crossing times.

One intriguing issue has to do with the time independence of the metric, which actually oscillates around or close to a certain fixed shape. In fact, due to the considerable amplitude of such oscillations it is possible to imagine that probably the evolved configuration corresponds to another configuration with different properties than those of the initial data. In Fig. 3 two different cases that are representative are shown: in the first case, the maximum of the metric function γ_{xx} oscillates around the right value calculated with the 1D code, which is assumed to be the correct value; in the second case the maximum of the metric component

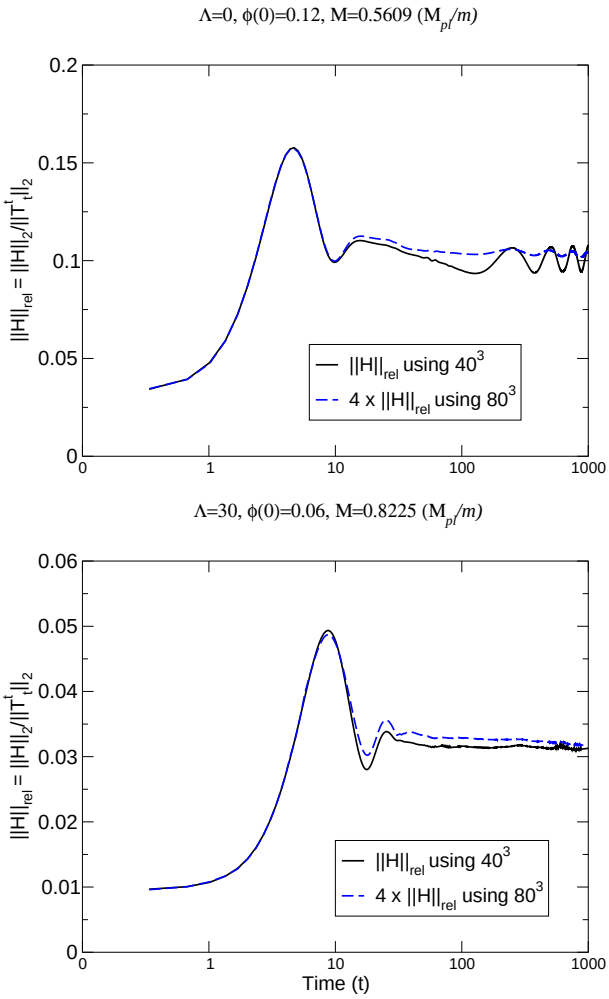

FIG. 2: Convergence of the relative L2 norm of the hamiltonian constraint for two configurations; the normalization factor is the $T^t{}_t$ component of the stress energy tensor. The resolutions used were $\Delta xyx = 0.675$ for the 40^3 box and $\Delta xyz = 0.3375$ for the 80^3 box in each of the configurations.

oscillates, but not around the expected value, instead with smaller values all the way. The fact is that in both cases the oscillating values of $max(\gamma_{xx})$ converge to a constant value that coincides with the one calculated at initial time. The second order convergence of this quantity indicates that the desired configuration is the one being evolved.

C. Radial Modes

With high spatial resolution it is quite easy to obtain very small variations of the metric functions in time, but since one is dealing with a coarse 3D grid the situation is slightly different. Instead, due to the errors introduced when populating the 3D grid with the initial data and those due to the discretization, one is dealing with perturbed configurations and thus it is possible to see only how the geometry converges to a fixed one when the spatial resolution is increased. Nevertheless I take advantage of this fact now to study oscillating radial modes as done in [11], but in the present case using the 3D code.

When studying the 1D problem with very refined grids it was necessary to set up an explicit perturbation by adding particles or kinetic energy to the initial equilibrium configuration in order to study the oscillations of the space time [11] [1]. Taking advantage of having a coarse grid, one gets for free the errors introduced when setting up the initial data, plus the discretization errors due to the numerical methods, act as a spherical perturbation, since an equally spaced grid is used in all directions, so that the evolution starts with perturbed configurations that converge to a strict equilibrium configuration, and it is possible to follow the oscillations of the metric functions. An indication that the perturbations applied are spherical consists in showing the amplitude of the Zerilli function extracted from the evolutions for the case of an unequally spaced grid in the z-direction as shown below.

In Fig. 4 appear the results found for equilibrium configurations evolved for three different values of self-interaction. Each point represents a run on a 40^3 (the coarse grid here) in octant mode of one of the equilibrium configurations indicated in Fig 1, which was run up to $t \geq 1000$ in coordinate time and stopped because of two factors: a) even if the evolution algorithm used is less dissipative than the usual second order ones, dissipation starts being noticed and b) the phase of the scalar field also starts to be shifted and begins to be less good. The frequency of the modes shown was calculated as usual $f = 1/T/\alpha(\infty_{grid})$ where T is the period of the maximum of the metric functions and ∞_{grid} is the outermost point of the grid. The curves shown in Fig. 4 mimic those found for these same configurations obtained with a 1D code [11]. An important difference between the method used in [11] and the used here is that in the former case the system was perturbed with a shell of particles falling towards the star, and in the present case the discretization error is used as the perturbation. In the first situation the metric functions oscillate with an amplitude that approaches exponentially towards their values corresponding to the unperturbed configuration, and in the present case no extra particles are added, which implies that there is no extra matter to be ejected, and no exponential decay of the amplitude of the oscillations is expected, instead, the discretization error is present over all the numerical

[1] Nevertheless this author has measured the same effects without the need of perturbing the number of particles and just taking care of the perturbations due to the discretization errors in a personal 1D code.

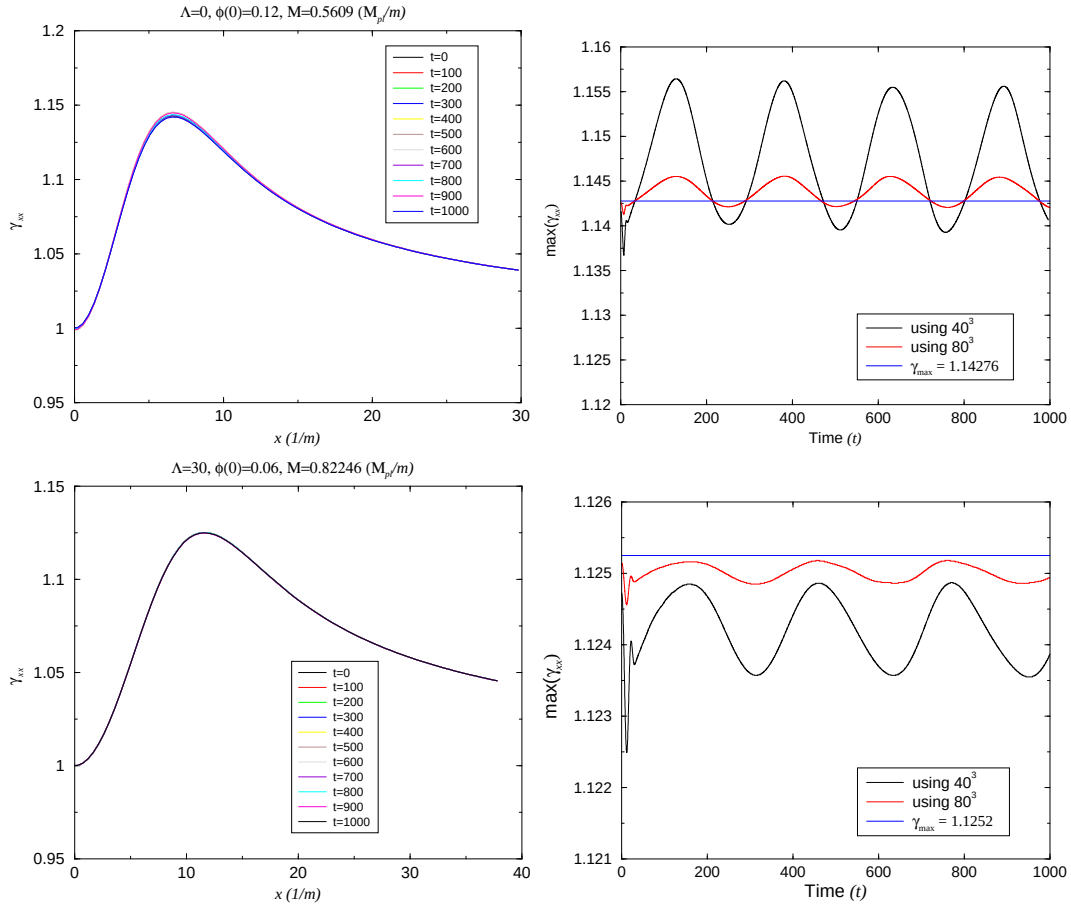

FIG. 3: On the left, the γ_{xx} metric function is shown for different systems evolved on an 80^3 grid and the highest resolution mentioned in the previous figure. On the right is shown the shape of the maximum of γ_{xx} in time and its second order convergence to the constants $max(\gamma_{xx}) = 1.14276$ and $max(\gamma_{xx}) = 1.12525$, which correspond to the values for each of the two configurations calculated at initial time with high resolution using a 1D code.

domain at every time.

IV. THE UNSTABLE BRANCH

Unstable boson star configurations are equilibrium configurations characterized by the fact that even using very fine tuned initial data and very high resolution, the finite differencing error in the calculations suffices to make the star collapse or disperse. In order to analyze the physical properties of unstable BSs I study in particular the case $\Lambda = 0$. An important feature of the unstable branch of BSs is the threshold related to the sign of the binding energy $E_B = M - Nm$, where N is the number of particles $N = \int \phi^* \phi$ and M is the mass measured by an observer at infinity. If $E_B < 0$ the system is expected to collapse and form a black hole, and otherwise the system is unstable due to the excess of energy translated into kinetic energy, and (like in a fission process) it should be dispersed into free particles at infinity [28], and this is precisely what is confirmed in

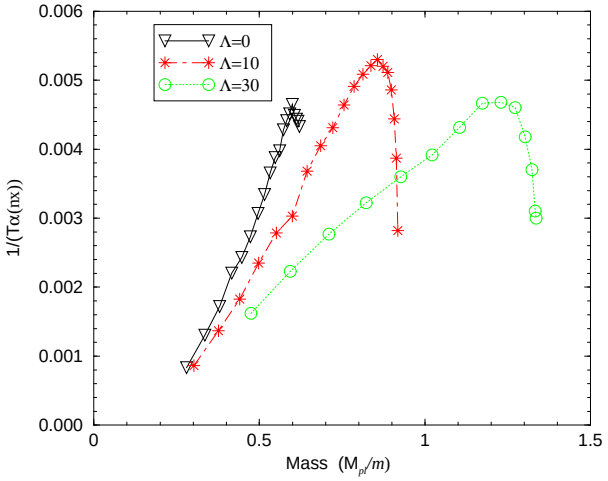

FIG. 4: The frequencies of oscillation of $\max(\gamma_{xx})$ for several equilibrium configurations is shown. It was found to be in very good agreement with those plots found with a 1D code for the same systems and others in reference [11]. Here I just present some cases corresponding to certain values of $\Lambda = \lambda/4\pi G m^2$.

these simulations[2]. The limiting situation $E_B = 0$ occurs for the case $\Lambda = 0$ when $\phi(0) = 0.54$. This threshold splits the unstable branch of equilibrium configurations into two regions: one corresponding to configurations with central field value $0.271 < \phi(0) < 0.54$, i.e. between the critical point $\phi(0) = 0.271$ separating the stable and the unstable branches and the threshold of zero binding energy $\phi(0) = 0.54$; the fate of the configurations belonging to this region is the formation of a black hole. The second region corresponds to configurations with $\phi(0) > 0.54$, which should disperse away.

In Fig. 5 a typical density evolution is presented for the case of a collapsing BS, both before and after the Black Hole is formed. After finding an apparent horizon for the first time, the excision is applied to all the variables that are being evolved and those serving to monitor the system (e.g. the energy-density). In the same figure the mass of the apparent and event horizons of the resulting black hole are shown. The discrepancy between the mass of the apparent and event horizons and the original mass of the system is within 0.4% after most of the matter has been absorbed, around $t \sim 90$. The event horizon is a concept that depends on the global structure of the space-time, therefore it can only be tracked in a post-process step after the simulation was finished. The event horizon finder [29] works by evolving null surfaces backwards in time using the information stored during the space-time evolution. Two initial surface guesses are necessary to start the event horizon tracking. One guess is chosen in a region outside and other inside the expected location of the horizon. These guesses were chosen based on the apparent horizon radius. The event horizon is at the end the surface the two initial guesses converge to. This is the reason why in Fig. 5 two different event horizon masses are shown. It can be seen that by the end of the simulation (the start of the event horizon tracking) the mass of the two initial surfaces does not coincide, and that around $t = 105$ the two measurements converge to a single one: the event horizon.

[2] In [10] it was found that independently of the sign of the binding energy, the configurations belonging to the unstable branch collapse into black holes for the case $\Lambda = 0$ studied here. In [11] however, it is confirmed that for $E_B > 0$ in the case of excited boson stars the configurations are dispersed away. In the present 3D case, due to the limitations on the numerical domain, it was not possible to confirm is after an expansion (far away from the 3D box) the system should have recollapsed to form a black hole, or if a migration to a very dilute configuration ocurred. In any case, it is a coincidence that stars with $\phi(0) > 0.54$ simply dispersed away, whereas those with $0.271 < \phi(0) < 0.54$ simply collapsed without any noticeable ejection of matter. An essential difference to be kept in mind is the nature of the perturbations applied here, where the number of particles is not being modified at all, and the perturbation is applied to the system across the whole numerical domain through discretization error

Based on these two important tools it is shown in Fig. 6 that the ratio of polar to equatorial circumferences is one over the evolution, indicating that the horizons are spherical, despite the lego-type shape of the excision boundary. This ratio will be fundamental in determining the physical parameters of the resulting black hole in the case of evolutions with fewer symmetries. E.g. from the oscillations of $C_r = C_p/C_e$ it is possible to obtain the angular momentum of a black hole resulting from the collapse of very general configurations (see e.g. [30, 31]). Finally, in Fig. 7 the evolution of T^t_t for a dispersing BS is presented, where the ejection of matter is manifest.

V. EXCITING NON-RADIAL MODES

Since the systems presented here have spherical symmetry, no gravitational wave signals are expected. Nevertheless as an exercise and in order to show that the modes studied in section III were actually radial, I take advantage of the freedom one has in 3D to apply a simple trick just by choosing different spatial resolutions $\Delta x = \Delta y \neq \Delta z$ with the consequent effect that the system is being perturbed in the z direction, and thus gravitational radiation is obtained in the fundamental mode simply due to discretization error. The perturbation consisted in using a grid size $40 \times 40 \times 35$ in the x, y, z directions respectively and resolution such that $\Delta x = \Delta y$, Δz was chosen so that the range in the three directions was the same. In Fig. 8 the waveform for the fundamental mode $l = 2$, $m = 0$ are shown and compared with the results found for an isotropic grid. The wave forms were extracted with the methods described in [32]. The convergence of the wave forms is second order, and as expected it converges to zero, since in the continuum limit it is expected the grid to be isotropic and no signal in this mode could come out from a spherically symmetric source. In this way it is also shown that the modes analyzed in the section III were actually radial.

VI. FEATURES OF THE CODE

A. Restrictions

The period of time that the convergence is preserved acts as an indicator of the consistency properties of the scheme, formulation, and boundary conditions working all together. The runs were stopped at the times shown in the plots because: a) the convergence was not manifestly second order with the passage of time, b) the period of the scalar field drifted after a finite time. These problems could be sorted out just by using higher resolution in time; all the simulations were carried out using a CFL factor of $\Delta t/\Delta x = 0.05$ (which means

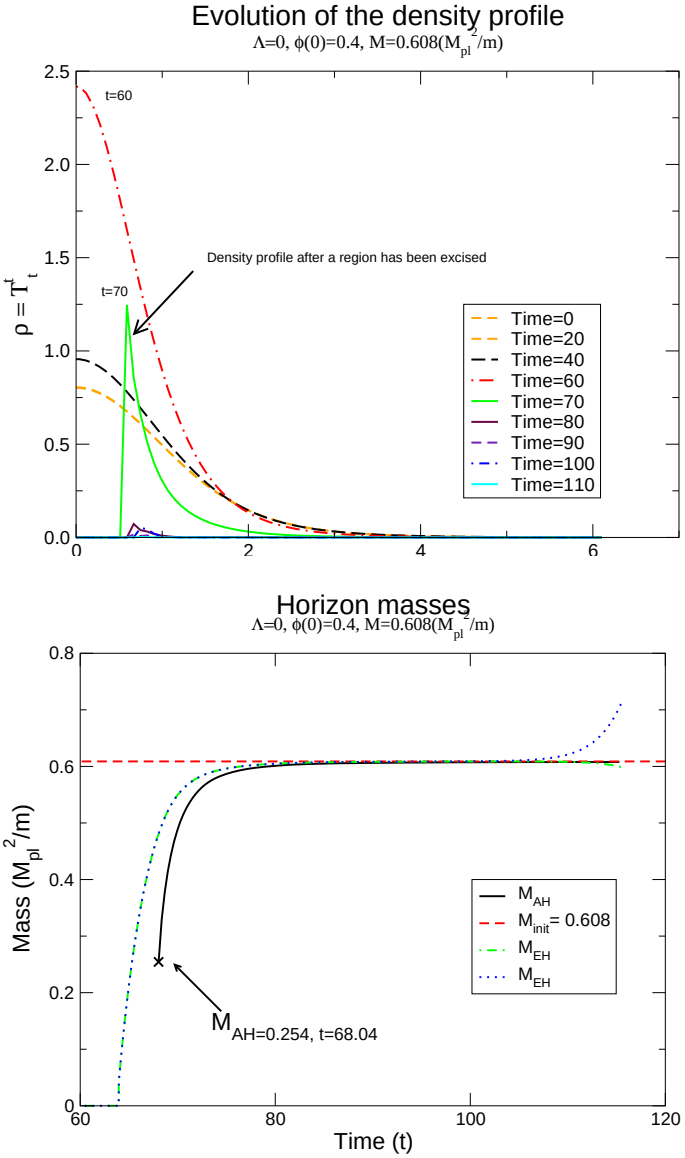

FIG. 5: In the top panel the evolution of the energy density is shown. At the first stage of the evolution (between $t = 0$ and 20) the density remains time independent; nevertheless after $t \sim 40$ the distribution starts concentrating close to the origin, and after $t \sim 64$ the system collapses and an event horizon is formed. Then around $t \sim 68$ an apparent horizon is found, after which excision is applied. At later times the remaining matter outside the horizon keeps falling into it. In the bottom panel the mass of the apparent horizon (M_{AH}), the event horizon (M_{EH}) and the initial total mass (M_{init}) are compared. After $t = 90$ and towards the end of the simulation the discrepancy is less than 0.4% between M_{EH} and M_{init}; a zoom in would show that the M_{AH} is always less than M_{EH}. The point marked with a cross indicates the moment at which an apparent horizon appears, after which, the increase in its mass is due to the accretion of the scalar field remaining outside. The two lines indicating the mass of an event horizon should be understood as follows: an interior and an exterior initial guesses for tracking the event horizon are chosen, thus it is expected they converge to two different null surfaces at the beginning of the tracking (that is, at the end of the simulation); however we know that when these null surfaces coincide the event horizon has been hunted; therefore the event horizon starts being tracked at around $t = 105$. The configuration corresponds to $\Lambda = 0$ and $\phi(0) = 0.4$, which is a typical case of the simulations collapsing into a black hole. The gauge parameters in (10) are $p = 2$ and $\eta = 0.25$. The evolution was performed with resolution $\Delta xyz = 0.07875$ in an 80^3 box in octant mode. The simulation was stopped at around $t \sim 117$ due to an instability coming from the inner boundary.

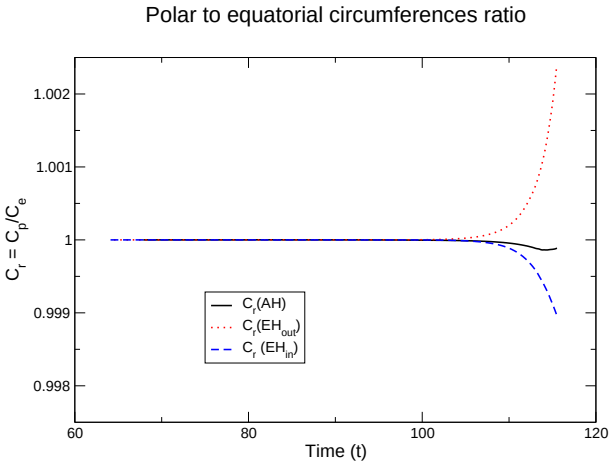

FIG. 6: The polar to equatorial circumference ratio is shown for the different horizons, and it is manifest that their shape is spherical within an error of 0.2% towards the end of the simulation.

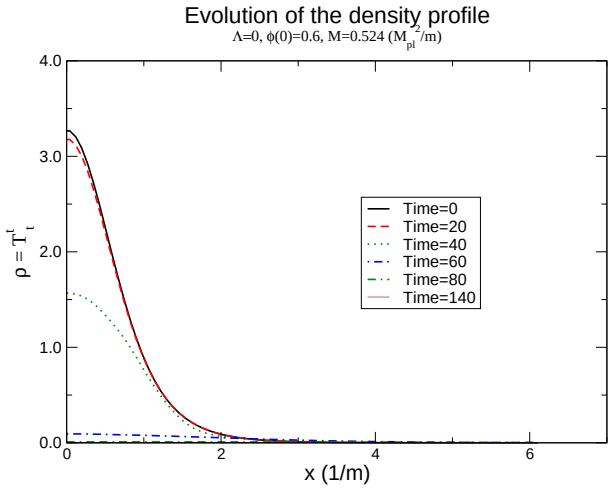

FIG. 7: The energy density profile of the configuration $\Lambda = 0$ and $\phi(0) = 0.6$ is shown at different stages. Due to the restricted domain it could happen either that the system should recollapse after traveling a distance outside the box to form a black hole as claimed in [10], or it is confirmed the fact that for configurations with positive binding energy the system truly disperses away and never recollapses. This controversy is expected to be solved once the present code is able to use notably bigger domains with the help of mesh refinement techniques. The configuration corresponds to $\Lambda = 0$ and $\phi(0) = 0.6$. The gauge parameters and resolution are the same as those used for the collapsing system shown above.

that the runs required tens of thousands of iterations), but convergence and period could be preserved just by decreasing such number. Another reason to choose such a small value of the CFL factor was that it helps at diminishing dissipation after a very long time of evolution.

Another issue is the problem of resolution. During

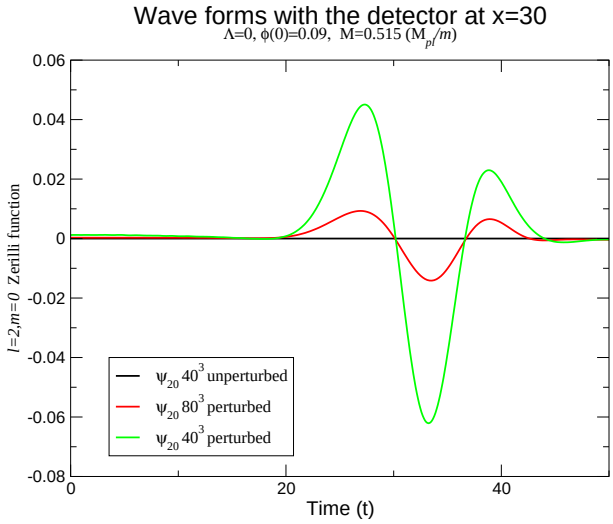

FIG. 8: The wave form and its convergence is shown for the fundamental mode with a detector located at $x = 30(1/m)$. The perturbed system was $\Lambda = 0$, $\phi_1(0, 0) = 0.09$ and $M = 0.51533(M_{pl}/m)$. The solid line around zero is the amplitude of the wave form when the system is evolved on the isotropic grid.

the evolutions presented in this manuscript there were at most a couple of dozens of points (using the low resolution) covering the volume containing 95% of the total mass of the star, and twice as much outside such region. In consequence the gravitational wave detectors had to be placed rather close to the BS. But even so, the results are good. The ideal situation for more general configurations would be: high resolution in the central part of the grid and a physical domain big enough to allow one to place detectors far away from the source. Thus practically means that the detector would be located in a Schwarzschild-like region thus providing cleaner signals.

Using a uniform grid works fine for spherical symmetry, but presents a dilemma in other cases: use high resolution to cover the central part and then forget about obtaining high quality waveforms, or conversely, sacrifice the resolution at the center and pull the grid far away in order to have a clean gravitational wave signal, but produced by a not accurately evolved source. The solution to this problem would be provided by the implementation of mesh refinement [33, 34, 35], and will be useful when dealing with systems under more interesting symmetries.

B. Restrictions on the physics

The phase of the field is an important indicator of the control one has on the simulation, because if the field is out of phase or the period of oscillation of the field

are not the right ones, then the effects will be noticed in the geometric quantities. Among the experiments carried out, it was observed that when using a three step iterative Crank-Nicholson (3ICN) [36] or second order Runge-Kutta (RK2) methods to evolve the system, the period of the scalar field changed after a while ($t \sim 200$), whereas the third order Runge-Kutta preserved the phase and the period, although a modified version of ICN [37] proved to work properly as well.

The dissipation is another issue one has to deal with when evolving matter. By observing the amplitude of the scalar field it was found that after $t \sim 1000$ the 3ICN provided an amplitude of the field $\sim 10\%$ less than the original one, while with the RK2 the amplitude of the field it was 15% bigger than the right value for the resolutions used here, which effects were evident in the measurement of physical quantities. The amplitude of the field after $t \sim 1000$ was less than the original by 0.3% using the coarse resolution. Thus, the RK3 was the one providing the most confident results in terms of convergence for longer time, dissipation, phase and period of oscillation of the solutions. It was also essayed the fourth order Runge-Kutta scheme, however it required more time iterations and no major improvement in accuracy was found. RK3 showed to be optimal in performance and accuracy for the purposes of the runs shown here.

In the case of stable configurations, the duration time scale of the simulations was enough to observe the oscillations of a wide range of stable configurations. However, the expected period of oscillation for very diluted configurations (those to the left in Fig. 4) is bigger if the mass is smaller. Therefore, it was not possible to study those configurations within the ranges of evolution times achieved with the present resolution and evolution times at the moment.

In the case of unstable configurations it is not expected to observe a constant amplitude of the scalar field, instead the squeezing of the scalar field, which is confined to a small region, implies an increase in the amplitude of the field and energy density whereas it is more concentrated in a small region where nodes can be observed before the formation of an apparent horizon. After excision is applied, the gradients of the scalar field become important in the region close to the inner boundary, and some unstable modes develop at some point. We are certain these modes are not numerical artifacts because increasing the resolution they last more time to show up. I expect to report about this point in further reports.

VII. COMMENTS AND CONCLUSIONS

I have presented a 3D code that is able to keep under control the unconstrained evolution of spherically symmetric Boson Stars, both stable and unstable using the BSSN formulation of General Relativity, the $1 + \log$ slicing condition, a coarse grid and simple discretizations on a uniform grid and well known numerical methods to evolve in time.

Stable configurations were evolved during several crossing times with second order convergence of the hamiltonian constraint and some characteristic properties of the geometry, like the convergence of the maximum of the radial metric function to the appropriate value. The process of collapse of unstable configurations was followed for quite a long time of around $t \sim 80M$, after the BH was formed, with error in the mass of the horizons of less than 0.4% in several cases studied. The configurations that dispersed where followed for a very long time and no surprises were found when evolving the resulting flat space-time.

It has been shown that these evolution techniques work properly when the IVP is not solved in the grid used for the evolution. This procedure will permit one to distinguish future problems intrinsically related to the solution of the initial value problem directly on the 3D grid [38]. I also decided to use simple uniform grids in order to set up test beds for future Boson Star simulations without involving coordinate transformations [39] that will be used for further research or mesh refinement that will be helpful as well [33].

It is possible to conclude by stating that it has been possible to reproduce in a 3D cartesian grid, the basic results found with 1D codes for spherically symmetric Boson Stars, which are related to infinitesimal perturbations due to the discretization error. In addition, taking advantage of the freedom one has in 3D grids to choose the discretization error in different directions, it was possible to extract a wave form that illustrates the type of signals one could expect from BSs and showed that the signal obtained when exciting the fundamental mode, presents a quick damping as predicted for axial perturbations of Boson Stars [40].

A comment about the late development of a 3D code for boson stars is in turn. Under the ADM formulation of General Relativity [41] it was rather difficult to evolve a Boson Star in 3D for the periods of time shown here (see e.g. [7]). The main reason preventing such long evolution was the ADM formulation itself, which showed to be inefficient at evolving a garden variety of physical systems [7]. On the other hand, at the present time one accounts with several new gauge conditions allowing the control of the simulations. A few years ago considerable effort was invested to evolve Boson Stars in 3D that did

not succeed only because of the formulation used [42, 43], although previous studies using new formulations were also explored [44]. It is necessary to point out that now it is possible to study in depth the phenomenology of Boson Stars in full 3D with the new techniques and tools that are emerging in the field of numerical relativity. Boson Stars could still be systems helpful at testing new numerical techniques, but most important they can be considered objects whose existence could eventually be probed if they are thought to be sources of gravitational waves.

This code was written as a thorn in the Cactus frame, and can be plugged into the variety of analysis tools and drivers available in the Cactus toolkit [45].

Acknowledgments

The author thanks Horst Beyer, Peter Diener, Ian Hawke, Ed Seidel, Arturo Ureña and Jason Ventrella for important comments and suggestions; special thanks to Ian Hawke for implementing the MoL thorn, Jonathan Thornburg for implementing the apparent horizon finder, Peter Diener for implementing the event horizon finder, and the Cactus-team for providing the necessary development tools. The Cactus and CactusEinstein infrastructure with AEI thorns were extensively used. The simulations were carried out in the Peyote cluster at the AEI and in the SuperMike cluster at LSU. This work was supported by the Center for Computation and Technology at LSU. This research was partly supported by the German-Mexican bilateral project DFG-CONACyT 444 MEX-13/17/0-1.

[1] R. Ruffini and S. Bonazolla, Phys. Rev. **187** (1969) 1767.
[2] D. J. Kaup, Phys. Rev. **172** (1968) 1331.
[3] M. Colpi, S. L. Shapiro and I. Wasserman, Phys. Rev. Lett. **57** (1986) 2485.
[4] Jae-weon Lee, In-guy Koh, Phys. Rev. **D 53** (1996) 2236. E. W. Mielke and F. E. Schunck, Phys. Rev. **D 66** (2002) 023503. F. S. Guzmán and L. A. Ureña-López, Phys. Rev. **D 68** (2003) 024023.
[5] D. F. Torres, S. Capozziello, G. Lambiase Phys. Rev. **D 62** (2000) 104012.
[6] F. D. Ryan, Phys. Rev. **D 55** (1997) 6081.
[7] M. Alcubierre, B. Bruegmann, T. Dramlitsch, J. A. Font, P. Papadopoulos, E. Seidel, N. Stergioulas and R. Takahashi, Phys. Rev. **D 62** (2000) 044034.
[8] P. Jetzer, Phys. Rep. **220** 4 (1992) 163.
[9] F. E. Schunck and E. W. Mielke, Class. Quantum Grav. **20** (2003) R301.
[10] E. Seidel and W-M. Suen, Phys. Rev. D **42**, 384 (1990);
[11] J. Balakrishna, E. Seidel, and W-M. Suen, Phys. Rev. D **58**, 104004 (1998).
[12] S. H. Hawley and M. W. Choptuik, Phys. Rev. **D 62** (2000) 104024.
[13] M. Shibata and T. Nakamura, Phys. Rev. **D 52** (1995) 5428. T. W. Baumgarte and S. L. Shapiro, Phys. Rev. **D 59** (1999) 024007.
[14] M. Alcubierre, G. Allen, B. Brügmann, E. Seidel and W-M Suen, Phys. Rev. **D 62** (2000) 124011.
[15] M. Alcubierre *et al.*, Class. Quantum Grav., **21** (2004) 589.
[16] E. W. Mielke and R. Scherzer, Phys. Rev. **D 24** (1981) 2111.
[17] T. D. Lee and Y. Pang, Phys. Rep. **221** (1992) 251.
[18] J-W Ho, S-J Kim and B-H Lee, gr-qc/9902040.
[19] F. E. Schunck and D. F. Torres, Int. J. Mod. Phys. **D 9** (2000) 601.
[20] R. J. LeVeque, *Numerical Methods for Conservation Laws*. Series, Birkhäuser Verlag, Basel, 1990.
[21] M. Alcubierre and B. Bruegmann, Phys. Rev. **D 63** (2001) 104006.
[22] M. Alcubierre, B. Bruegmann, P. Diener, M. Koppitz, D. Pollney, E. Seidel and R. Takahashi, Phys. Rev. **D 67** (2003) 084023.
[23] M. Alcubierre, B. Bruegmann, D. Pollney, E. Seidel and R. Takahashi, Phys. Rev. **D 64** (2001) 061501.
[24] H.J. Yo, T. W. Baumgarte and S. L. Shapiro, Phys. Rev. **D 64** (2001) 124022.
[25] M. D. Duez, S. L. Shapiro, W-J Yo, gr-qc/0401076.
[26] L. Baiotti, I. Hawke, P .J. Montero, F. Loeffler, L. Rezzolla, N. Stergioulas, J. A Font, E. Seidel, gr-qc/0403029.
[27] J. Thornburg, Class. Quantum Grav. **21** 2 (2004) 743.
[28] M. Gleiser, Phys. Rev. **D 38** (1988) 2376.
[29] P. Diener, Class. Quantum Grav. **20** (2003) 4901.
[30] S. Brandt and E. Seidel, Phys. Rev. **D 52** (1995) 856.
[31] M. Alcubierre, B. Bruegmann, P. Diener, F. S. Guzmán, I. Hawke, F. Herrmann, M. Koppitz, D. Pollney, E. Seidel and J. Thornburg, in preparation.
[32] G. Allen, K. Camarda and E. Seidel, gr-qc/9806014 and gr-qc/9806036.
[33] E. Schnetter, S. H. Hawley and I. Hawke, Class. Quantum Grav. **21** (2004) 1465.
[34] B. Imbiriba *et al.*, gr-qc/0403048.
[35] S. L. Liebling, gr-qc/0403076.
[36] S. Teukolsky, *Phys. Rev. D* **61**, 087501 (2000).
[37] M. Alcubierre, R. Becerril, F. S. Guzmán, T. Matos, D. Núñez and L. A. Ureña-López, Class. Quantum Grav., **20** (2003) 2883.
[38] J. Balakrishna, R. Bondarescu, G. Daues, F. S. Guzmán and E. Seidel, in preparation.
[39] J. Baker, M. Campanelli and C. Lousto, Phys. Rev. **D 65** (2002) 044001.

[40] S. Yoshida, Y. Eriguchi and T. Futamase, Phys. Rev. **D 50** (1994) 6235.
[41] J. York, *Sources of Gravitational Radiation*, Ed by Larry L. Smarr. Cambridge University Press, Cambridge, 1979.
[42] D. I. Choi, Ph D Thesis, The University of Texas at Austin 1998.
[43] J. Balakrishna, Ph D Thesis, Washington University 1999. E-version: gr-qc/9906110.
[44] T. Dramlitsch, Masters Thesis, Universität Potsdam, 1999.
[45] B. Bruegmann, Ann. Phys. (Leipzig) **9**, 3-5 (2000) 227. E. Seidel and W-M Suen, JCAM **109** (1999) 493. **http://www.cactuscode.org**